Controlling Spontaneous Emission from Perovskite Nanocrystals with Metal-Emitter-Metal Nanostructures

Liliana Tjahjana[1,2], Kwan Lee[1,2], Xin Yu Chin[3], Landobasa Y.M. Tobing[2], Gede W.P. Adhyaksa[3], Dao Hua Zhang[2], Muhammad Danang Birowosuto[1,2]*, Hong Wang[1,2]*

[1] CINTRA (CNRS-International-NTU-THALES Research Alliances/UMI 3288), Research Techno Plaza, 50 Nanyang Drive, Border X Block, Level 6, Singapore 637553, Singapore; ltjahjana@ntu.edu.sg (L.T.)

[2] School of Electrical and Electronic Engineering, Nanyang Technological University, 50 Nanyang Avenue, Singapore 639798, Singapore

[3] Energy Research Institute @ NTU (ERIAN), Research Techno Plaza, 50 Nanyang Drive, X-Frontiers Block, Level 5, Singapore 637553, Singapore

* Correspondence: ewanghong@ntu.edu.sg (H.W.); mbirowosuto@ntu.edu.sg (M.D.B.); Tel.: +65-6790-6595 (M.D.B.)

Abstract: We show the enhancement in the intensity and emission rate of perovskite cesium lead bromide ($CsPbBr_3$) and formamidinium lead bromide ($FAPbBr_3$) nanocrystals in the presence of single and double gold layer cavities, which we refer to as Metal-Emitter (ME) and Metal-Emitter-Metal (MEM) nanostructures. Up to 1.9-fold photoluminescence intensity and up to 5.4-fold emission rate enhancements were obtained for $FAPbBr_3$ nanocrystals confined by double gold layers, which are attributed to plasmonic confinement from the gold layers. The experimentally obtained values are validated by analytical calculations and electromagnetic simulations. Such an effective method of manipulation of the spontaneous emission rate by simple plasmonic nanostructures can be utilized in sensing and detection applications.

Keywords: perovskite; nanocrystal; Purcell effect

1. Introduction

Metal halide perovskites for quantum emitter have gained interest over the years due to their low cost and solution-processable characteristics [1]. Importantly, the defect-tolerant characteristics of halide perovskites are responsible for their high absorption coefficients and high photoluminescence quantum yield, enabling potential large-scale applications in photovoltaic (PV) devices [2], scintillators [3-6], light-emitting diodes (LEDs), lasers, photodetectors, and field-effect transistors (FETs) [7]. Moderate exciton binding energy in the several meV range, large oscillator strength, and tuneable bandgap achieved via tailoring of chemical composition and structural diversity are the other advantages of halide perovskite, notably in nonlinear optics applications [8] and strong light-matter interaction between quantum emitter and optical cavity.

Coupling electromagnetic modes with quantum emitter [9, 10] results in the emission rate modification known as the Purcell effect, which is relevant for realizing single-photon nano-emitters [11]. The light-confining structures can be realized via different platforms, such as photonic crystals [12, 13], disorder [14, 15], and plasmonic nanostructures [16]. In this work, we investigate the spontaneous emission rate modification of halide perovskite nanocrystals coupled with simple plasmonic cavities. The quantum emitters investigated in this work are cesium lead bromide ($CsPbBr_3$) and formamidinium lead bromide ($FAPbBr_3$) nanocrystals (NC), while the plasmonic cavity is defined in metal-emitter (ME) and metal-emitter-metal (MEM) structures in which the nanocrystals are sandwiched between single and double gold films, respectively. We obtained 1.2-fold and 1.9-fold intensity enhancement for $CsPbBr_3$ and $FAPbBr_3$ nanocrystals respectively; whereas

the emission rate enhancements are 4.3-fold and 5.4-fold for $CsPbBr_3$ and $FAPbBr_3$ nanocrystals respectively. Manipulation of the spontaneous emission rate by simple plasmonic nanostructures can be utilized in sensing and detection applications [17, 18].   Furthermore, such simple structures with large emission enhancement factors will improve the brightness for light-emitting devices (LED) applications and improve the signal modulations in telecommunication technologies.

2. Materials and Methods

The schematic of the ME and MEM structures are shown in Figure 1(a). The 100-nm thick bottom gold layer was physically deposited on glass substrate by electron beam evaporation. To avoid non-radiative losses, a thin polystyrene (PS) layer was deposited in between gold and perovskite layer. PS layer was spin coated from PS in toluene solution (1.5% w/v) at 8000rpm to obtain initial thickness of 35nm, followed by oxygen plasma etching (450mBarr, 30-50s) to reach 15 nm thickness. $CsPbBr_3$ NC was synthesized according to a hot-injection protocol described in the literature [5, 19]. In a typical synthesis, 0.7 g lead (II) bromide ($PbBr_2$), oleic acid (0.5 mL), oleyl amine (0.5 mL) and octadecene (5 mL) were loaded into a 50 mL flask and dried under vacuum at 100 °C for 0.5 h. Subsequently, nitrogen (N_2) was introduced and the mixture was heated up to 170 °C until $PbBr_2$ was completely dissolved. A hot Cs-oleate precursor (0.5 mL) was quickly injected into the flask under vigorous stirring. After 10 s of reaction, the flask was quickly immersed into an ice bath to quench the reaction. The $CsPbBr_3$ NC precipitate was collected by centrifugation for 10 mins. The NC suspension was then spun on the cover slide at 4000 rpm for 10 seconds (for 100 nm thickness) and at 6000 rpm for 10 seconds (for 50 nm thickness) with initial volumes of 0.1 and 0.05 ml, respectively. $FAPbBr_3$ NC was synthesized and spin coated by methods described in Chin et al [20].
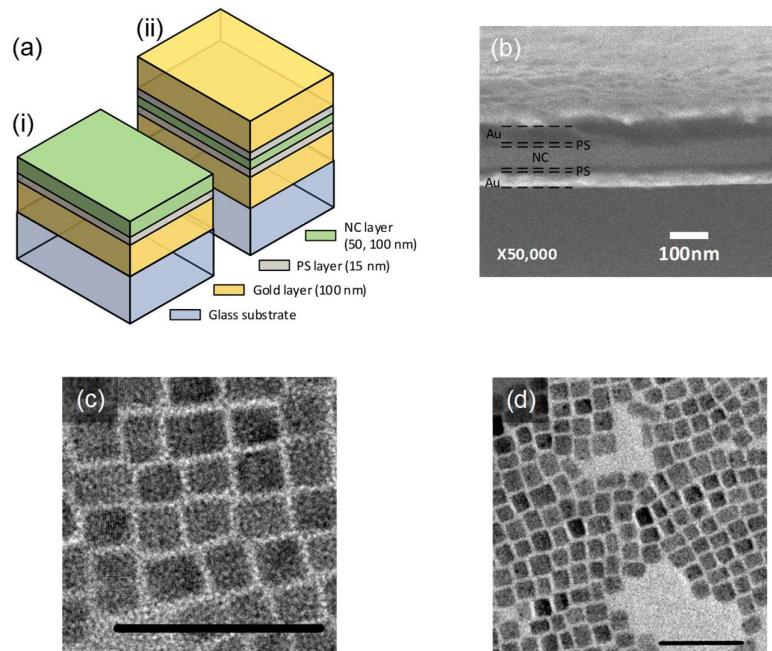
Figure 1.(**a**) Schematic of i) single- and ii) double-Au-PS layers with $CsPbBr_3$ or $FAPbBr_3$ nanocrystals ; (**b**) Scanning electron micrograph of the cross section of 50-nm $CsPbBr_3$ nanocrystals, double 15-nm PS films, and double-Au layers; TEM pictures of (**c**) $CsPbBr_3$ and (**d**) $FAPbBr_3$ nanocrystals, with black scale bar indicating 50nm.

PL measurements were performed at room temperature using free-space excitation and collection through a visible–near-infrared microscope objective (Nikon 20×, NA = 0.40).   The sample was excited via a 10 MHz picosecond pulsed diode laser (Master Oscillator Fibre Amplifier, Picoquant, excitation wavelength at 355 nm, pulse width 50 ps, and power of 40 µW). The PL

measurement was based on epifluorescence method. PL spectra were detected using AvaSpec-HERO spectrometer. The emission was then filtered by a linear variable filter at 505 and 545 nm and detected by a single-photon avalanche photodiode connected to a time-correlated single-photon counting acquisition module (Edinburgh Instruments, TCC900). The time-resolved photoluminescence (TRPL) decay curves were fitted with two exponential functions. The average lifetime was calculated from the decay time components and amplitudes of the fitted TRPL decay curves.

For double gold structure, another gold layer was evaporated on another PS layer on top of the perovskite NC layer to 100nm thickness. The scanning electron micrograph (SEM) of the double gold structure is shown in Figure 1(b), with each layer indicated accordingly. The thicknesses of the layers are verified from Scanning Electron Microscopy (SEM) images with the cross-section thicknesses analysed statistically (an example is shown in Figure S1 in Supplementary Information). The transmission electron micrograph (TEM) pictures of the $CsPbBr_3$ and $FAPbBr_3$ nanocrystals are shown in Figures 1(c) and 1(d) respectively.

3. Results and Discussion

Figure 2 presents the photoluminescence (PL) spectra of $CsPbBr_3$ and $FAPbBr_3$ nanocrystals in different scenarios. We varied the thickness of the NC layer to 50nm and 100 nm for the two nanocrystals and normalized the PL spectra to those of the reference (dashed black curves). The reference is PS-NC-PS system (Figure S2 in Supplementary Information). The emission wavelengths are found at 505nm (for $CsPbBr_3$ NC) and 545 nm (for $FAPbBr_3$ NC). For each experimental data point, the photoluminescence and decay measurements were performed at two positions of 5mm apart on the same sample, and the average and standard deviation of the results were taken. The normalized PL spectra of NC in metal-emitter situation are shown in red curves, showing intensity enhancement of ~1.13 and ~1.41 times for $CsPbBr_3$ and $FAPbBr_3$ nanocrystals of 50-nm thickness, respectively. Here, 15-nm thick PS layer is introduced between the gold film and the NC layer to minimize non-radiative loss. The non-radiative loss associated with metals is commonly attributed to the energy transfer from excited electrons to the free carriers inside the metal. Inserting a thin insulating layer would reduce such non-radiative loss [21-23]. Stronger resonance is expected when a second gold layer is introduced. The resonance characteristics of ME and MEM structures were verified in the thickness-dependent peak positions in the transmittance measurement (see Figure S3 in Supplementary Information). Normalized PL spectra of NC in metal-emitter-metal situation are shown in blue curves, showing PL intensity enhancements of ~1.23 (for $CsPbBr_3$ NC) and ~1.91 (for $FAPbBr_3$ NC) of 50-nm thickness.
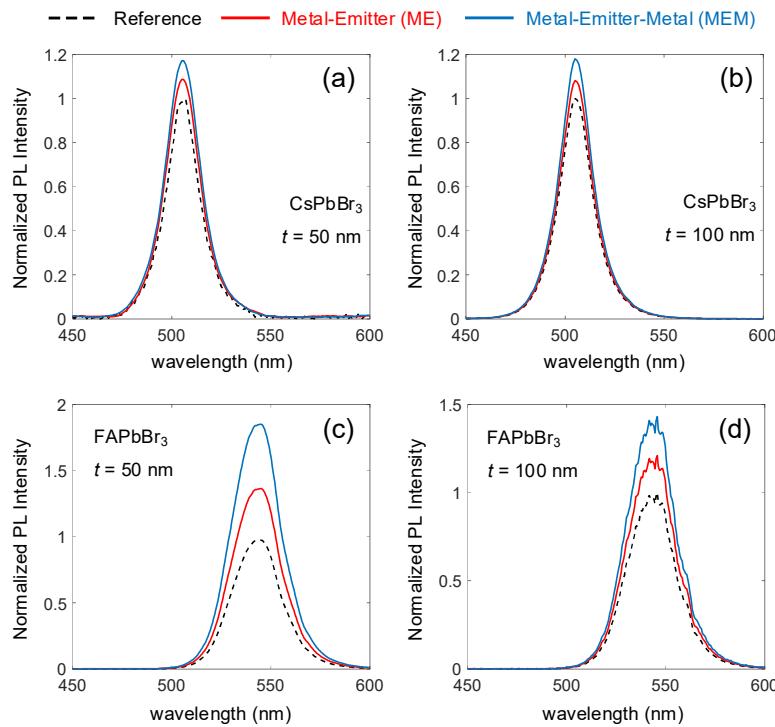
Figure 2. Photoluminescence (PL) spectra of NC-PS-Au layers at room temperature (RT) with CsPbBr₃ nanocrystals of (**a**) 50- and (**b**) 100-nm thick; and FAPbBr₃ nanocrystals of (**c**) 50- and (**d**) 100-nm thick. The black dashed, red solid, and blue solid lines correspond to reference, single-Au-PS, and double-Au-PS layers, respectively.

As both the gold film(s) and the NC layer form the plasmonic cavity, with light confinement within the NC layer, the role of the NC layer is thus expected on the resonance condition. This is illustrated when the NC layer thickness is increased to 100 nm, presented in Figure 2(b) and Figure 2(d) for CsPbBr₃ and FAPbBr₃ nanocrystals, respectively. While the PL intensity enhancement remains relatively unchanged for CsPbBr₃ nanocrystals, it decreases from ~1.41 to ~1.21 (for metal-emitter configuration) and from ~1.91 to ~1.42 (for metal-emitter-metal configuration) for FAPbBr₃ nanocrystals. By the same reasoning, the resonance condition is also dependent on the thickness of the PS spacer layer. This means that the PS layer serves not only to minimize non-radiative loss, but also to modify the resonance condition of the plasmonic cavity. The PL characteristics of NC layer without PS spacer layer is shown in Figure S4 (Supplementary Information), indicating strong decrease in emission intensity, which has also been observed before [24]. Time-resolved photoluminescence characteristics for all scenarios are presented in Figure 3, showing spontaneous emission rate modification as the nanocrystals are coupled in metal-emitter or metal-emitter-metal configurations. Since both intensity and emission rate are enhanced, as shown in Table 1, this indicates Purcell effect taking place in both types of nanocrystals. To verify the role of PS spacer layer in Purcell effect, we present in Figure S5 (Supplementary Information) the time-resolved PL measurements of 50-nm thick CsPbBr₃ NC on gold film without PS spacer layer. We found that the fast decay component in this situation is very close to the instrument response function (IRF) of about 0.3 ns [23]. Coupled with the intensity decrease in Figure S1, it is seen that the fast decay rate is not attributed to Purcell effect, but to non-radiative loss instead. Therefore, while there is a reduction of non-radiative recombination by PS, the plasmonic/dielectric cavity are still the key driving force which enhances the emission rate.
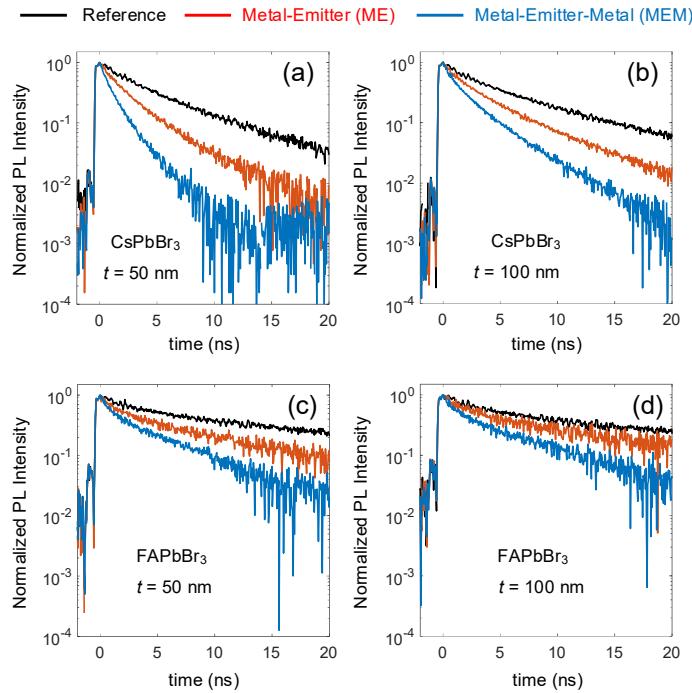
Figure 3. Time-resolved emission measurements. Decay curves of reference (black), single-Au-PS- (red), and double-Au-PS-NC samples (blue) measured for (**a**) 50- and (**b**) 100-nm-thick CsPbBr₃ nanocrystals and (**c**) 50- and (**d**) 100-nm-thick FAPbBr₃ nanocrystals. For measurements of CsPbBr₃ and FAPbBr₃ nanocrystals, we monitor 505- and 545-nm emission, respectively.

Table 1. Intensity and emission rate enhancements in metal-emitter and metal-emitter-metal configurations

Perovskite NC	Intensity enhancement (average ± standard deviation)		Emission rate enhancement (average ± standard deviation)	
	single	double	single	double
CsPbBr₃ (50nm)	1.13 ± 0.11	1.23 ± 0.12	2.00 ± 0.57	4.28 ± 0.57
CsPbBr₃ (100nm)	1.08 ± 0.11	1.18 ± 0.11	1.76 ± 0.62	2.92 ± 0.63
FAPbBr₃ (50nm)	1.41 ± 0.14	1.91 ± 0.19	2.42 ± 0.66	5.38 ± 0.67
FAPbBr₃ (100nm)	1.21 ± 0.12	1.42 ± 0.14	1.75 ±0.66	4.18 ± 0.67

To further understand the experimental results, we turn to analytical calculation and then validate it with finite element simulation (FEM) in COMSOL. The metal-emitter and metal-emitter-metal configurations can be modelled as a set of thin-film stacks with different optical permittivity values and the nanocrystals as dipoles within the NC layer, as denoted by the red dots, as shown in Figure 4(a). The orientation of the electric dipole is such that it gives emission in the XY plane. Using the Fresnel reflections, the spontaneous emission rate modification of a dipole in metal-emitter configuration can be calculated as [25-28]

$$F_P = \frac{\Gamma_T}{\Gamma_0} = 1 - \frac{3}{2} Q_e \, \text{Im} \int_0^\infty R_p^{1,2,3}(k_2, t) \exp(-2l_1 d) \frac{u^3}{l_1} du, \tag{1}$$

where F_P is the spontaneous emission rate enhancement factor, Q_e is the quantum efficiency, d is the dipole distance from the interface of metal layer, t is the thickness of the metal layer, k is the propagation constant, $l_m = -i\sqrt{\epsilon_m/\epsilon_1 - u^2}$, $R_p^{1,2,3}$ is the total p-polarized reflection from the thin film stack

$$R_p^{1,2,3}(k_2, t) = \frac{R_p^{1,2} + (R_p^{2,3} \cdot e^{-2l_2 k_2 t})}{1 + R_p^{1,2} \cdot (R_p^{2,3} \cdot e^{-2l_2 k_2 t})}, \tag{2}$$

with $R_p^{m,n} = \frac{\epsilon_m l_n - \epsilon_n l_m}{\epsilon_m l_n + \epsilon_n l_m}$ denoting *p*-polarized Fresnel reflection between *m*th and *n*th layer. The subscripts 1, 2, and 3 refers to perovskite nanocrystal layer, gold layer, and glass substrate, respectively. For an electric dipole in metal-emitter-metal configuration, the emission rate modification is

$$F_P = \frac{\Gamma_T}{\Gamma_0} = 1 - \left[Q_e \cdot \left(1 - \frac{3}{2} \text{ Im} \int_0^\infty \frac{\left(1 - R_p^{1,2,3}(k_2,t)e^{-2l_1k_1 d}\right)\left(1 - R_p^{1,2,3}(k_2,t)e^{-2l_1k_1(L-d)}\right)}{\left(1 - (R_p^{1,2,3}(k_2,t))^2 e^{-2l_1k_1 L}\right)} \frac{u^3}{l_1} du \right) \right], \quad (3)$$

where the subscripts 1, 2, and 3 refers to perovskite nanocrystal layer, gold layer, and air, respectively.

The graphs next to the schematics in Figure 4(a) illustrate the change in spontaneous emission rate enhancement over dipole distance from metal surface. At the centre of the perovskite film ($d = 0.5L$), the spontaneous emission rate enhancement factor (F_P) for double gold layer structure is approximately two times of that of the single gold case, in range of $L \lesssim 0.5\lambda$. The quantum efficiency of the perovskite nanocrystals is assumed to be $Q_e = 0.4$ [19, 20], while their permittivity values were obtained from spectroscopic ellipsometry, as shown in Figure 4(b). We note that the refractive index values of the FAPbBr3 appear to be lower than others reported elsewhere. This is attributed to the organic ligands protecting the surface of FAPbBr3 nanocrystals, which makes it behaves more like a composite rather than thin-film crystal [20].
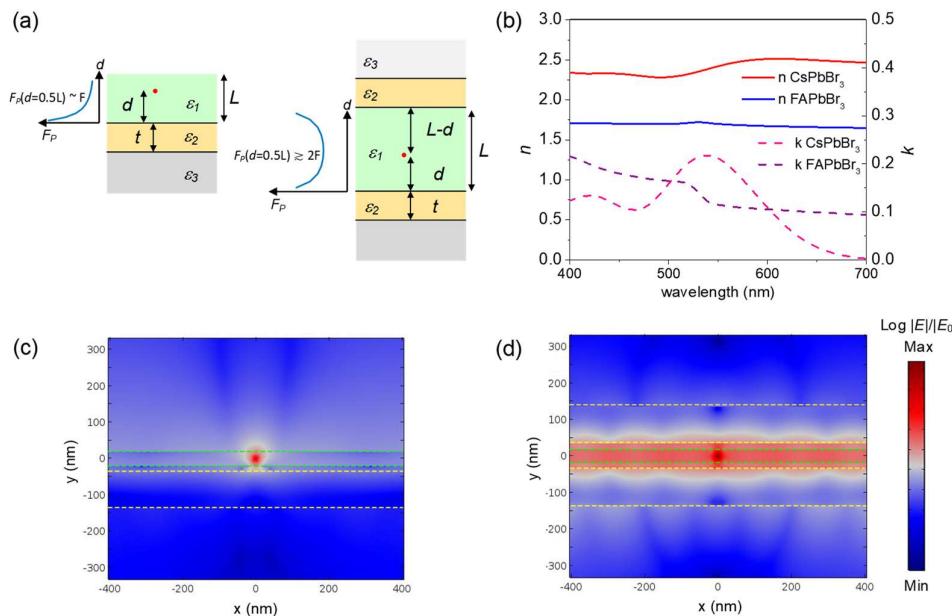
Figure 4. Analytical calculation and electromagnetic simulation approaches to determine the emission rate enhancement: (**a**) Geometry of single and double finite films for analytical calculation and electromagnetic simulation of fluorescence near an interface. Some variables in the scheme are explained in the text. The graphs illustrate the change in spontaneous emission rate enhancement factor (F_P) over dipole distance from metal surface; (**b**) Experimental optical constants obtained from variable angle spectroscopic ellipsometry for CsPbBr3 and FAPbBr3 NC film; Electric field intensity enhancement mapping for a point dipole in the middle of 50-nm-thick CsPbBr3 film (**c**) on the top of one Au-PS layer and (**d**) sandwiched between two Au-PS layers at 540nm and 606 nm resonance wavelength, respectively. The structures are indicated by dashed lines.

In the finite element simulation [23, 29], the emission rate enhancement is calculated as the dipole power ratio between that within the plasmonic layer structures and that in the perovskite film only. The calculated $|E|$-field mappings at resonances for ME and MEM structures with CsPbBr3 NC film are shown in Figure 4(c) and Figure 4(d), respectively. The resonant wavelengths were found from simulation to be at 540nm for ME structure and 606nm for MEM structure. The resonant wavelength is the optical characteristic of the layer structure, obtained from FEM simulation, which

is not related to the emission wavelength of the nanocrystals, although ideally the emission and resonant wavelengths should coincide so that the final enhancement is at maximum. In addition, the peaks and the long wavelength shifts of the resonances from 50- and 100-nm MEM structures well agree with the transmittance measurements of Figure S3 in Supplementary Information. The NC layer is denoted by the green dashed lines, while the gold films are indicated by the yellow dashed lines. The optical modes are confined differently in the two configurations. The *E*-field for the ME case is localized at the vicinity of the electric dipole, while the *E*-field for the MEM case is rather extended in the transverse direction, mimicking that of a waveguide. This translates to stronger light-matter interaction in the MEM case, which gives higher emission rate modification.

The comparison among the calculated, simulated, and measured emission rates for the two nanocrystals with 50-nm and 100-nm thicknesses is presented in Figure 5. For the calculation and FEM simulation in this work, the emission rate is averaged over more than 10 equally spaced points over the entire perovskite NC layer thickness. We found that our analytical results and FEM simulations are in good agreement with our experimental results. The difference is due to the boundary problem between PS and NC layers in both simulations. For $FAPbBr_3$ NC, up to 1.9-fold PL intensity and up to 5.4-fold emission rate enhancements were observed for the case of 50nm thick NC layer in double gold layer structure.
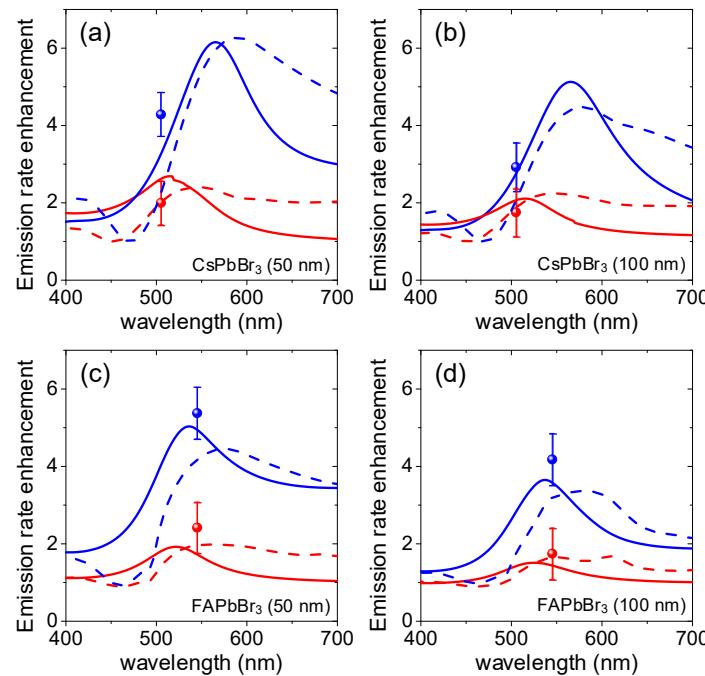
Figure 5. Emission rate enhancement comparison between measurements and calculations. Experimental values (spheres) and calculations of emission rate enhancement from the analytical (solid lines) and the electromagnetic simulations (dashed lines) of fluorescence near the interface from single-Au-PS (red) and double-Au-PS (blue) layers with (**a**) 50nm-thick $CsPbBr_3$ NC film, (**b**) 100-nm thick $CsPbBr_3$ NC film, (**c**) 50nm-thick $FAPbBr_3$ NC film, (**d**) 100-nm thick $FAPbBr_3$ NC film.

We note that the intensity enhancement of $FAPbBr_3$ nanocrystals is higher than that of $CsPbBr_3$ nanocrystals. This can be attributed to the inter-band transition of gold at 539 nm [30, 31], suggesting that the gold layer behaves more as dielectric at wavelengths shorter than its inter-band transition. Indeed, this appears to be the case for $CsPbBr_3$ nanocrystals whose emission wavelength is at 505 nm (< 539 nm). However, the light is still confined by virtue of total internal reflection. This is because the real refractive index of gold is 0.887 at 505 nm [30]. Considering the real refractive index of $CsPbBr_3$ NC is 2.3 at 505nm, the index contrast of ~1.4 is large enough for ensuring optical confinement within the NC layer. Considering the ~20nm emission linewidth of $CsPbBr_3$ NC, the

enhancement is attributed more to dielectric confinement rather than plasmonic confinement. This is in contrast with FAPbBr$_3$ nanocrystals, whose emission wavelength (545 nm) is longer than the inter-band transition of gold. Considering its emission linewidth of ~30 nm, the light confinement is dominated more by plasmonic mechanism rather than by total internal reflection. This also agrees with more pronounced enhancements in FAPbBr$_3$ nanocrystals compared to CsPbBr$_3$ nanocrystals.

4. Conclusions

The intensity and emission rate characteristics of CsPbBr$_3$ and FAPbBr$_3$ nanocrystals have been investigated in two metal-emitter configurations. Owing to their emission wavelengths with respect to the inter-band transition of gold, the enhancements in the two nanocrystals are attributed to different mechanisms. For CsPbBr$_3$ NC, whose emission wavelength is shorter than gold inter-band transition, the gold behaves more as dielectric and the light is confined by virtue of strong index contrast. For FAPbBr$_3$ nanocrystals, whose emission wavelength is longer than gold inter-band transition, the light is confined by plasmonic mechanisms. These confinement mechanisms are the reason for the big differences in the intensity and emission enhancements of the two nanocrystals. By treating the metal-emitter and metal-emitter-metal configurations as thin film stacks, we arrived at the analytical formulation to elucidate the emission enhancement, which was also validated by our FEM simulation. We found good agreement between our calculation and our experimental results. In addition, we have shown that a simple plasmonic cavity based on single or double gold films can be used as a platform to study light-matter interaction, particularly in solution-processable perovskite NC, which can be used for sensing application [17, 18].

Other metals can be explored in the future. Silver should perform better compared to gold due to its much lower damping loss and its inter-band transition at the ultraviolet spectrum. However, unlike gold, silver is known to suffer from surface oxidation, which deteriorates its plasmonic response with time. The other good candidate is aluminium (Al), which is known to support plasmonic resonance in the UV-Vis spectrum. Moreover, its surface oxidation is known to be self-limiting in the 2-3 nm thickness range, which can also serve to minimize non-radiation loss as the PS layer in our work. Although Al damping loss is known to be higher than gold or silver, Al is an excellent candidate for plasmonics in the ultraviolet spectrum, making it suitable platform for quantum emitter in the short-visible wavelength range.

Supplementary Materials: Figure S1: Example of statistical analysis of layer thickness; Figure S2: Schematic of reference sample in PL and TRPL measurements, Figure S3: Transmittance of metal-emitter and metal-emitter-metal structures; Figure S4: Photoluminescence (PL) spectra of CsPbBr$_3$ NC-Au layers (without PS) at room temperature (RT); Figure S5: Time-resolved emission of CsPbBr$_3$ NC film with Au, Table S1: Key parameters of time resolved PL spectrum;

Author Contributions: Conceptualization, M.D.B.; formal analysis, M.D.B., L.T., L.Y.M.T.; investigation, M.D.B., L.T.; resources, K.L, G.W.P.A. and C.X.Y.; data curation, M.D.B., L.T.; writing—original draft preparation, M.D.B., L.T.; writing—review and editing, L. Y.M. T, G.W.P.A.; visualization, M.D.B., L.T., L.Y.M.T.; supervision M.D.B., H.W. and Z.D.H. All authors have read and agreed to the published version of the manuscript.

Funding: This research was funded by Ministry of Education, Singapore, grant nos. MOE2016-T2-1-052 and MOE2019-T1-002-063.

Acknowledgments: We acknowledge Aozhen Xie for assistance in CsPbBr$_3$ NC synthesis.

Conflicts of Interest: The authors declare no conflict of interest.

References

1.   Dai, Xingliang, Zhenxing Zhang, Yizheng Jin, Yuan Niu, Hujia Cao, Xiaoyong Liang, Liwei Chen, Jianpu Wang, and Xiaogang Peng. "Solution-Processed, High-Performance Light-Emitting Diodes Based on Quantum Dots." *Nature* 515, no. 7525 (2014): 96-99.

2.   Abate, Antonio, Juan-Pablo Correa-Baena, Michael Saliba, Mohd Sukor Su'ait, and Federico Bella. "Perovskite Solar Cells: From the Laboratory to the Assembly Line." *Chemistry – A European Journal* 24, no. 13 (2018): 3083-100.

3.   Birowosuto, M. D., D. Cortecchia, W. Drozdowski, K. Brylew, W. Lachmanski, A. Bruno, and C. Soci. "X-Ray Scintillation in Lead Halide Perovskite Crystals." *Sci. Rep.* 6 (2016): 37254.

4.   Xie, Aozhen, Tien Hoa Nguyen, Chathuranga Hettiarachchi, Marcin E. Witkowski, Winicjusz Drozdowski, Muhammad Danang Birowosuto, Hong Wang, and Cuong Dang. "Thermal Quenching and Dose Studies of X-Ray Luminescence in Single Crystals of Halide Perovskites." *J. Phys. Chem. C* 122, no. 28 (2018): 16265-73.

5.   Chen, Qiushui, Jing Wu, Xiangyu Ou, Bolong Huang, Jawaher Almutlaq, Ayan A. Zhumekenov, Xinwei Guan, Sanyang Han, Liangliang Liang, Zhigao Yi, Juan Li, Xiaoji Xie, Yu Wang, Ying Li, Dianyuan Fan, Daniel B. L. Teh, Angelo H. All, Omar F. Mohammed, Osman M. Bakr, Tom Wu, Marco Bettinelli, Huanghao Yang, Wei Huang, and Xiaogang Liu. "All-Inorganic Perovskite Nanocrystal Scintillators." *Nature* 561, no. 7721 (2018): 88-93.

6.   Birowosuto, M. D., P. Dorenbos, C. W. E. van Eijk, K. W. Krämer, and H. U. Güdel. "Scintillation and Luminescence Properties of Ce3+ Doped Ternary Cesium Rare-Earth Halides." *physica status solidi (a)* 204, no. 3 (2007): 850-60.

7.   Zhou, Chenkun, Haoran Lin, Qingquan He, Liangjin Xu, Michael Worku, Maya Chaaban, Sujin Lee, Xiaoqin Shi, Mao-Hua Du, and Biwu Ma. "Low Dimensional Metal Halide Perovskites and Hybrids." *Materials Science and Engineering: R: Reports* 137 (2019): 38-65.

8.   Wu, Leiming, Keqiang Chen, Weichun Huang, Zhitao Lin, Jinlai Zhao, Xiantao Jiang, Yanqi Ge, Feng Zhang, Quannan Xiao, Zhinan Guo, Yuanjiang Xiang, Jianqing Li, Qiaoliang Bao, and Han Zhang. "Perovskite Cspbx3: A Promising Nonlinear Optical Material and Its Applications for Ambient All-Optical Switching with Enhanced Stability." *Advanced Optical Materials* 6, no. 19 (2018): 1800400-00.

9.   Gholipour, Behrad, Giorgio Adamo, Daniele Cortecchia, Harish N. S. Krishnamoorthy, Muhammad. D. Birowosuto, Nikolay I. Zheludev, and Cesare Soci. "Organometallic Perovskite Metasurfaces." *Adv. Mater.* 29, no. 9 (2017).

10.   Hou, Songyan, Aozhen Xie, Zhenwei Xie, Landobasa Y. M. Tobing, Jin Zhou, Liliana Tjahjana, Junhong Yu, Chathuranga Hettiarachchi, Daohua Zhang, Cuong Dang, Edwin Hang Tong Teo, Muhammad Danang Birowosuto, and Hong Wang. "Concurrent Inhibition and Redistribution of Spontaneous Emission from All Inorganic Perovskite Photonic Crystals." *ACS Photonics* 6, no. 6 (2019): 1331-37.

11.   Hou, Songyan, Muhammad Danang Birowosuto, Saleem Umar, Maurice Ange Anicet, Roland Yingjie Tay, Philippe Coquet, Beng Kang Tay, Hong Wang, and Edwin Hang Tong Teo. "Localized Emission from Laser-Irradiated Defects in 2d Hexagonal Boron Nitride." *2D Mater.* 5, no. 1 (2017): 015010.

12.   Birowosuto, M. D., A. Yokoo, G. Zhang, K. Tateno, E. Kuramochi, H. Taniyama, M. Takiguchi, and M. Notomi. "Movable High-Q Nanoresonators Realized by Semiconductor Nanowires on a Si Photonic Crystal Platform." *Nat. Mater.* 13, no. 3 (2014): 279-85.

13.   Birowosuto, M. D., A. Yokoo, H. Taniyama, E. Kuramochi, M. Takiguchi, and M. Notomi. "Design for Ultrahigh-Q Position-Controlled Nanocavities of Single Semiconductor Nanowires in Two-Dimensional Photonic Crystals." *Journal of Applied Physics* 112, no. 11 (2012): 10.

14.   Birowosuto, M. D., S. E. Skipetrov, W. L. Vos, and A. P. Mosk. "Observation of Spatial Fluctuations of the Local Density of States in Random Photonic Media." *Phys. Rev. Lett.* 105, no. 1 (2010).

15. Sapienza, Luca, Henri Thyrrestrup, Søren Stobbe, Pedro David Garcia, Stephan Smolka, and Peter Lodahl. "Cavity Quantum Electrodynamics with Anderson-Localized Modes." *Science* 327, no. 5971 (2010): 1352.

16. Farahani, J. N., D. W. Pohl, H. J. Eisler, and B. Hecht. "Single Quantum Dot Coupled to a Scanning Optical Antenna: A Tunable Superemitter." *Phys. Rev. Lett.* 95, no. 1 (2005): 017402.

17. Gökbulut, Belkıs, Ekrem Yartaşı, Ezgi Sunar, Ozlem Ipek Kalaoglu-Altan, Tugce Nihal Gevrek, Amitav Sanyal, and Mehmet Naci Incı. "Humidity Induced Inhibition and Enhancement of Spontaneous Emission of Dye Molecules in a Single Peg Nanofiber." *Optical Materials Express* 8, no. 3 (2018): 568-80.

18. Gökbulut, Belkıs, Arda Inanç, Gokhan Topcu, Tugrul Guner, Mustafa M. Demir, and M. Naci Inci. "Enhancement of the Spontaneous Emission Rate of Perovskite Nanowires Coupled into Cylindrical Hollow Nanocavities Formed on the Surface of Polystyrene Microfibers." *The Journal of Physical Chemistry C* 123, no. 14 (2019): 9343-51.

19. Protesescu, Loredana, Sergii Yakunin, Maryna I. Bodnarchuk, Franziska Krieg, Riccarda Caputo, Christopher H. Hendon, Ruo Xi Yang, Aron Walsh, and Maksym V. Kovalenko. "Nanocrystals of Cesium Lead Halide Perovskites (Cspbx3, X = Cl, Br, and I): Novel Optoelectronic Materials Showing Bright Emission with Wide Color Gamut." *Nano Lett.* 15, no. 6 (2015): 3692-96.

20. Chin, Xin Yu, Ajay Perumal, Annalisa Bruno, Natalia Yantara, Sjoerd A. Veldhuis, Laura Martínez-Sarti, Bevita Chandran, Vladimir Chirvony, Alencious Shu-Zee Lo, Jinkyu So, Cesare Soci, Michael Grätzel, Henk J. Bolink, Nripan Mathews, and Subodh G. Mhaisalkar. "Self-Assembled Hierarchical Nanostructured Perovskites Enable Highly Efficient Leds Via an Energy Cascade." *Energy Environ. Sci.* 11, no. 7 (2018): 1770-78.

21. Akselrod, Gleb M., Christos Argyropoulos, Thang B. Hoang, Cristian Ciracì, Chao Fang, Jiani Huang, David R. Smith, and Maiken H. Mikkelsen. "Probing the Mechanisms of Large Purcell Enhancement in Plasmonic Nanoantennas." *Nature photonics.* 8, no. 11 (2014): 835-40.

22. Hoang, Thang B., Gleb M. Akselrod, Christos Argyropoulos, Jiani Huang, David R. Smith, and Maiken H. Mikkelsen. "Ultrafast Spontaneous Emission Source Using Plasmonic Nanoantennas." *Nature Communications* 6, no. 1 (2015): 7788.

23. Saleem, Umar, Fitri A. Permatasari, Ferry Iskandar, Takashi Ogi, Kikuo Okuyama, Yudi Darma, Meng Zhao, Kian Ping Loh, Andrivo Rusydi, Philippe Coquet, Muhammad Danang Birowosuto, and Hong Wang. "Surface Plasmon Enhanced Nitrogen-Doped Graphene Quantum Dot Emission by Single Bismuth Telluride Nanoplates." *Advanced Optical Materials* 5, no. 17 (2017).

24. Dayal, Govind, Ankur Solanki, Xin Yu Chin, Tze Chien Sum, Cesare Soci, and Ranjan Singh. "High-Q Plasmonic Infrared Absorber for Sensing of Molecular Resonances in Hybrid Lead Halide Perovskites." *Journal of Applied Physics* 122, no. 7 (2017): 073101.

25. Drexhage, K. H. "Influence of a Dielectric Interface on Fluorescence Decay Time." *Journal of Luminescence* 1-2 (1970): 693-701.

26. Chance, R. R., A. Prock, and R. Silbey. "Molecular Fluorescence and Energy Transfer near Interfaces." *Advances in Chemical Physics* (1978): 1-65.

27. Barnes, W. L. "Electromagnetic Crystals for Surface Plasmon Polaritons and the Extraction of Light from Emissive Devices." *Journal of Lightwave Technology* 17, no. 11 (1999): 2170-82.

28. Jun, Y. C., R. D. Kekatpure, J. S. White, and M. L. Brongersma. "Nonresonant Enhancement of Spontaneous Emission in Metal-Dielectric-Metal Plasmon Waveguide Structures." *Physical Review B* 78, no. 15 (2008): 153111.

29.   Xu, Y., J. S. Vučković, R. K. Lee, O. J. Painter, A. Scherer, and A. Yariv. "Finite-Difference Time-Domain Calculation of Spontaneous Emission Lifetime in a Microcavity." *Journal of the Optical Society of America B* 16, no. 3 (1999): 465-74.

30.   Johnson, P. B., and R. W. Christy. "Optical Constants of the Noble Metals." *Physical Review B* 6, no. 12 (1972): 4370-79.

31.   Cooper, B. R., H. Ehrenreich, and H. R. Philipp. "Optical Properties of Noble Metals. Ii." *Physical Review* 138, no. 2A (1965): A494-A507.